JACS
JOURNAL OF THE AMERICAN CHEMICAL SOCIETY
Communication
pubs.acs.org/JACS

Single-Crystal and Electronic Structure of a 1.3 nm Indium Phosphide Nanocluster

Dylan C. Gary, Sarah E. Flowers, Werner Kaminsky, Alessio Petrone, Xiaosong Li, and Brandi M. Cossairt*

Department of Chemistry, University of Washington, Seattle, Washington 98195-1700, United States

Supporting Information

ABSTRACT: Magic-sized nanoclusters have been implicated as mechanistically relevant intermediates in the synthesis of group III-V quantum dots. Herein we report the single-crystal X-ray diffraction structure of a carboxylate-ligated indium phosphide magic-sized nanocluster at 0.83 Å resolution. The structure of this cluster, $In_{37}P_{20}(O_2CR)_{51}$, deviates from that of known crystal phases and possesses a non-stoichiometric, charged core composed of a series of fused 6-membered rings. The cluster is completely passivated by bidentate carboxylate ligands exhibiting predominantly bridging binding modes. The absorption spectrum of the cluster shows an asymmetric line shape that is broader than what would be expected from a homogeneous sample. A combination of computational and experimental evidence suggests that the spectral line width is a result of multiple, discrete electronic transitions that couple to vibrations of the nanocrystal lattice. The product of reaction of this nanocluster with 1 equiv of water has also been structurally characterized, demonstrating site selectivity without a drastic alteration of electronic structure.

Quantum-confined semiconductor nanocrystals (quantum dots, QDs) exhibit strongly size-dependent optical and electronic properties. As a result, considerable effort has been aimed at their integration into light-harvesting and -emitting devices both in the research laboratory and in the marketplace.[1,2] Predicting the properties of QDs requires detailed knowledge of their size, shape, and composition. A longstanding challenge in this field has been to prepare a homogeneous sample and to grow a single crystal in order to determine a high-resolution structure that allows for unambiguous assignment of these three properties. While there is a rich history of structural interrogation of transition metal and main group cluster molecules,[3−9] to date a complete, atomically precise structural picture of a binary semiconductor QD remains elusive.

Magic-sized nanoclusters have emerged as an important class of intermediates at the interface of small molecules and QDs.[10−17] As a class of truly monodisperse nanomaterials, magic-sized nanoclusters can offer unique insight into the structure of their larger QD counterparts. Several group II-VI magic-sized clusters have been identified and structurally characterized;[3,4,8] however, these clusters do not appear to be directly involved in the high-temperature nucleation of group II-VI QDs since their thermal instability precludes their buildup in these traditional syntheses where kinetics are readily controlled by precursor conversion chemistry.[18−21] For group III-V QDs, on the other hand, precursor conversion chemistry does not appear to be the rate-determining step in the overall growth mechanism,[12,22,23] and magic-sized clusters have been implicated as kinetically persistent intermediates whose thermal transformation may be an important step in QD nucleation.[12,24,25] Given the potential significance of these cluster intermediates in elucidating the mechanism of III-V QD formation and in understanding the physical and electronic structure of carboxylate-terminated QDs, we sought to isolate and structurally characterize one such cluster.

Herein, we report the first single-crystal X-ray diffraction (XRD) structure of an indium phosphide (InP) magic-sized nanocluster with 0.83 Å resolution, including all ligands. This nanocrystal ($In_{37}P_{20}(O_2CCH_2Ph)_{51}$) exhibits a non-stoichiometric core, a geometry that does not correspond to that of bulk InP, and unanticipated ligand binding modes. The electronic structure of $In_{37}P_{20}(O_2CCH_2Ph)_{51}$ is determined using a combination of spectroscopic and time-dependent density functional theory (TDDFT) methods, providing an unprecedented understanding of the way in which the surface of these nanoclusters impacts their optoelectronic properties.

Solution-based syntheses of semiconductor nanocrystals typically yield an ensemble of particles that range in terms of size, shape, and surface composition. However, $In_{37}P_{20}(O_2CR)_{51}$ is the sole nanocrystalline product that we obtain from reaction of tris(trimethylsilyl)phosphine, indium acetate, and carboxylic acid at 100 °C, as evident from elemental analysis and ^{31}P NMR spectroscopy (see Supporting Information (SI)). This cluster has previously been identified by its spectroscopic signatures as a magic size in the growth profile of InP QDs.[12,24] Crystals suitable for single-crystal X-ray analysis were grown from a supersaturated solution of particles (R = CH_2Ph) in ethyl acetate and formed as yellow prisms.

Physical Structure—Core. The structure of $In_{37}P_{20}(O_2CCH_2Ph)_{51}$ (Figure 1) exhibits several unanticipated features that deviate from the conventional model of a nanoparticle. Binary semiconductor nanocrystals are typically envisioned as possessing a crystalline, stoichiometric core structure that corresponds to a known bulk phase and is unaltered during ligand exchange reactions post-synthesis.[26,27] Additionally, this core would be surrounded by a shell of neutral, datively bound ligands or by a shell of excess metal cations

Received: December 17, 2015
Published: January 19, 2016

DOI: 10.1021/jacs.5b13214
J. Am. Chem. Soc. 2016, 138, 1510−1513

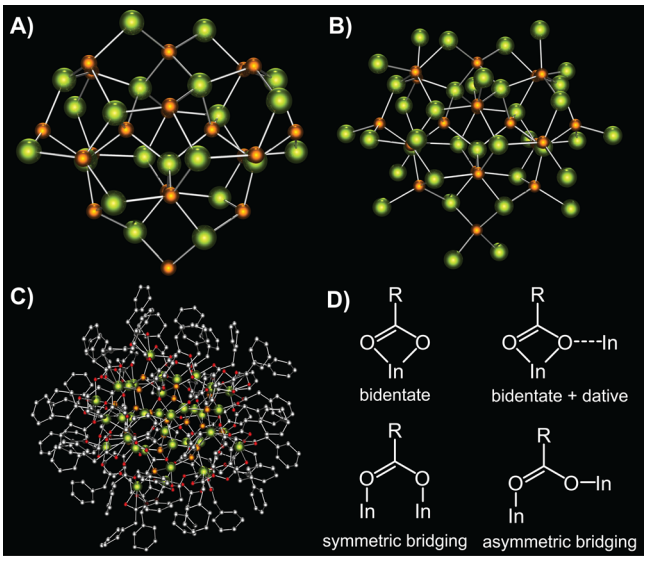

Figure 1. Molecular structure of $In_{37}P_{20}(O_2CCH_2Ph)_{51}$ (hydrogen atoms omitted for clarity). (A) $[In_{21}P_{20}]^{3+}$ core. (B) Core plus 16 surface indium atoms. (C) Complete single-crystal XRD structure including all ligands. (D) Schematic representation of all observed ligand binding modes. Of the 51 phenylacetate ligands, 12 are identified as bidentate, 1 is identified as bidentate + dative, 5 are identified as symmetric bridging, and 33 are identified as asymmetric bridging. Color legend: green, indium; orange, phosphorus; red, oxygen; gray, carbon.

charge-balanced by anionic ligands.[27,28] In the structure of $In_{37}P_{20}(O_2CCH_2Ph)_{51}$ there is no subset of atoms that can accurately be described as a stoichiometric, charge-neutral core of InP. The nanocrystal core, which consists solely of fused 6-membered rings with all phosphorus atoms coordinated to four indium atoms in a pseudo-tetrahedral arrangement (Figure 1A), has the formula $[In_{21}P_{20}]^{3+}$. This subset of atoms possesses a C_2 rotation axis that bisects two phosphorus atoms and a single indium atom located at the center of the particle, and measures approximately 1.3 nm × 1.0 nm × 1.0 nm. This arrangement of core atoms deviates from that of the known bulk phases of InP.[29] A dihedral angle of 160 ± 3° is consistent along the longest straight In−P chain and demonstrates a clear deviation from zincblende (ϕ = ±60° or ±180°) and wurtzite (ϕ = ±120°) (Figure S1). The average In−P bond length in the $[In_{21}P_{20}]^{3+}$ core is 2.528 Å (min 2.479 Å, max 2.624 Å), and the average P−In−P bond angle is 109.2° (min 97.7°, max 119.9°), while those of the zincblende lattice are 2.541 Å and 109.5°, respectively. An additional 16 indium atoms are singly bound to this core through surface-exposed phosphorus atoms (Figure 1B), with an average bond length of 2.482 Å (min 2.450 Å, max 2.515 Å). Since the sum of the single-bond covalent radii for In and P is 2.53 Å, it is inferred that the bonding in the inorganic core of this cluster may be best viewed as covalent in nature, with differences in bond lengths between In−P in the core and In−P at the surface arising from internal strain.[30]

Physical Structure—Surface. An accurate picture of the surface chemistry of InP nanoparticles is essential for understanding their optoelectronic properties and for designing methods to alter their surfaces post-synthetically, a crucial step for applications requiring high photoluminescence quantum yield or efficient charge extraction.[27,28,31−34] $In_{37}P_{20}(O_2CCH_2Ph)_{51}$ is an In-rich nanoparticle that is completely passivated by a phenylacetate ligand set with highly variable coordination modes (Figure 1C,D and Table S1). Each surface indium atom is bound to at least two other indium atoms through bridging carboxylate ligands, and as such this ligand set is best described as entirely anionic in nature (i.e., X-type), with no neutral, datively bound ligands.[27] This stands in contrast to the prevailing model of QD surfaces wherein the dominant coordination modes are thought to be labile, neutral Lewis bases such as primary amines acting as two-electron donors (L-type) or neutral Lewis acids acting as two-electron acceptors (Z-type).[28] Retention of this tightly bound and dense ligand packing in solution is confirmed via NMR spectroscopy. A $^1H-^1H$ COSY spectrum revealed that the methylene protons on a common carbon atom are chemically inequivalent, separated by up to 1.3 ppm. This large difference in chemical shift may be indicative of both hindered rotation about the C−C bonds of the methylene linker and CH−π interactions with nearby aromatic rings (Figure S2). Similar interactions have been observed for phenylalanine residues in small proteins.[35]

We discovered that single crystals of $In_{37}P_{20}(O_2CCH_2Ph)_{51}$ are sensitive to air exposure,[12] suggesting a chemical transformation of the particles under these conditions. When these crystals are exposed to air they begin to fracture within 30 min, and a change is observed in the dimensions of the unit cell. In a separate single-crystal XRD study on crystals exposed to moist air, we have identified a stoichiometric reaction with water wherein a single carboxylate ligand adopts a monodentate binding motif with the resulting open coordination site filled by a water molecule (Figure S3). This structural change has minimal impact on the frontier orbitals of the cluster, and hence its electronic structure shows little change, as indicated by TDDFT calculations (Figure S4). Interestingly, the reaction with water is selective for a single indium site (likely due to small differences in the Lewis acidity of the indium sites). This result suggests that stoichiometric and site-specific ligand chemistry may be achieved at the surfaces of semiconductor QDs.

To further illustrate the preference for complete saturation of the coordination sphere of the surface indium atoms (no "dangling bonds"), calculations were performed on a theoretical structure where a single bidentate carboxylate ligand was altered to act as a monodentate ligand. This structure is identical to the structure observed on exposure to water, but with the water ligand removed. The calculations from this model reveal that while the HOMO and HOMO-1 remain relatively unperturbed (*vide infra*), the LUMO has shifted such that the majority of the electron density is localized on the open coordination site of the under-coordinated indium atom (Figure S5). These calculations suggest that it is energetically favorable to saturate the coordination sphere of surface-bound In atoms and that the introduction of an open In coordination site (dangling bond) would manifest as a notable energetic separation of the HOMO-1−LUMO and HOMO−LUMO transitions, resulting in a more asymmetric peak shape in the absorption spectrum of the sample (Figure S6).

Electronic Structure. $In_{37}P_{20}(O_2CCH_2Ph)_{51}$ shows an asymmetric peak shape in the UV−vis spectrum for the lowest energy absorbance feature with maxima centered at 2.97 and 3.21 eV (Figure 2). TDDFT calculations predict this peak shape to be the result of a pair of energetically similar transitions, with the HOMO−LUMO transition assigned to the shoulder at 2.97 eV (418 nm) and the HOMO-1−LUMO transition assigned to the dominant peak at 3.21 eV (386 nm). These discrete electronic transitions, which are found at higher energies than in bulk InP (1.34 eV),[29] are typical of quantum-confined materials. For InP QDs, experimental data and theoretical predictions suggest that

DOI: 10.1021/jacs.5b13214
J. Am. Chem. Soc. 2016, 138, 1510−1513

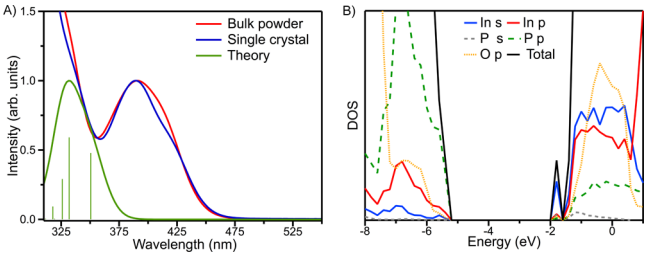

Figure 2. Optical spectra and density of states for $In_{37}P_{20}(O_2CCH_2Ph)_{51}$. (A) Experimental (blue, single crystal; red, bulk powder) and TD-HSE06/LANL2DZ computed (green) spectra obtained from the first 10 individual optical transitions (green vertical lines, see Table S4 crystal A) with a Gaussian smoothing function (width 0.12 eV). All intensities are normalized. (B) HSE06/LANL2DZ DOS and PDOS (see legend) diagram.

the size dependence of the band gap is best described by a $1/r$ relationship.[36−38] For a diameter of 1.3 nm, the $1/r$ model predicts a bandgap of 3.33 eV (372 nm),[37] which agrees favorably with our experimental observations.

At room temperature the lowest energy electronic transitions in $In_{37}P_{20}(O_2CCH_2Ph)_{51}$ are broad, with full widths at half-maximum of approximately 41 and 38 nm (Figure S7). Typically such broad peaks are thought to arise as a result of sample inhomogeneity, and synthetic efforts in the QD community have been directed at minimizing spectral line width through minimizing particle size and shape deviations.[26,39−41] In the absence of broadening from ensemble effects, spectral line widths tend to increase with a corresponding decrease in particle size.[42,43] Even though we have been able to prepare a homogeneous sample, we still observe a broader absorption line width than what has been reported for the intrinsic line width of nanocrystalline InP as well as for InP nanoclusters with a similar size.[12,44] We hypothesize that the major contributor to this line broadening is coupling with specific vibrational motions within the nanocrystal lattice that arises due to the localization of the frontier molecular orbitals of the particle (Figure 3). This

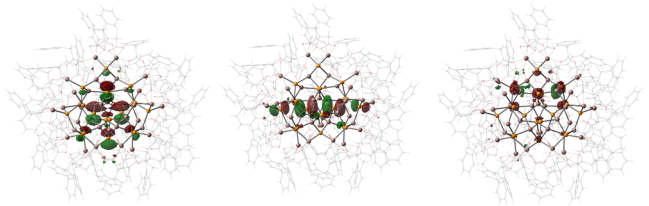

Figure 3. HSE06/LANL2DZ molecular orbital (MO) diagrams of the occupied (HOMO-1, left and HOMO, middle) and unoccupied (LUMO, right) orbitals involved in the most intense computed electronic transitions for $In_{37}P_{20}(O_2CCH_2Ph)_{51}$. The MOs were plotted with an isosurface value of 0.025.

hypothesis is supported by variable-temperature UV−vis spectroscopy, which shows significant spectral line narrowing and enhanced resolution of the HOMO−LUMO transition into a distinct peak as the sample is cooled to 100 K (Figure 4).

$In_{37}P_{20}(O_2CCH_2Ph)_{51}$ shows no appreciable photoluminescence at 298 K, consistent with observations of larger In-rich InP QDs, which typically exhibit photoluminescence quantum yields lower than 1%.[22,31] The primary non-radiative pathway proposed for InP nanocrystals is one where unpassivated surface atoms (dangling bonds) act as charge traps.[45] This is in line with observations that HF etching increases quantum yields up to 47%

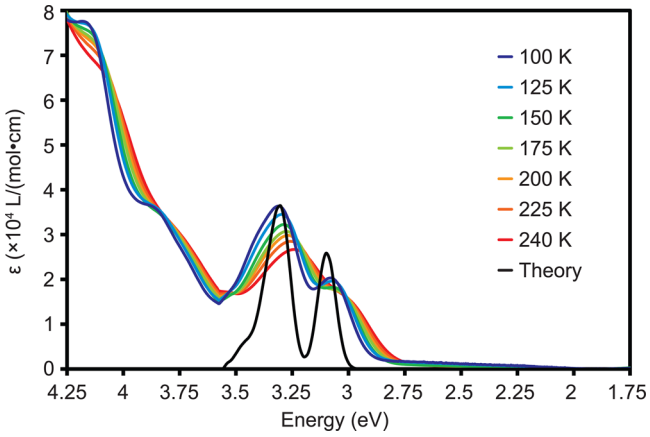

Figure 4. Experimental variable-temperature UV−vis spectra of $In_{37}P_{20}(O_2CCH_2Ph)_{51}$ in the solid state with a comparison to the TD-HSE06/LANL2DZ theoretical prediction obtained from the first 5 individual optical transitions smoothed by Gaussian functions (width 0.04 eV) and shifted and normalized to match the experimental peak maximum around 3.3 eV at 100 K.

by passivation of In dangling bonds with F^- and of P dangling bonds with H^+.[46] Additionally, EPR measurements of ground-state and photoexcited colloidal InP support the presence of both electron and hole traps.[47] Given that $In_{37}P_{20}(O_2CCH_2Ph)_{51}$ has neither unpassivated indium atoms nor phosphorus atoms at its surface, we hypothesize that the main energy loss pathway in this sample is through non-radiative vibrational relaxation due to motions within the crystal lattice.

In conclusion, we have characterized the physical and electronic structure of an indium phosphide magic-sized cluster, $In_{37}P_{20}(O_2CR)_{51}$, which is a key intermediate in the synthesis of InP quantum dots. Since this structure does not correspond to a known bulk phase or a magic number for a closed shell of valence electrons, it may be that the selectivity for and stability of this cluster can be attributed to the dense, interconnected network of supporting ligands passivating the particle surface. Not only does this result allow us insight into the structure of III-V QDs and nanocluster intermediates, it also leads us to propose several new structural principles to the field of semiconductor QDs. First, the cores of semiconductor nanocrystals need not be stoichiometric (neutral), as is seen for the $[In_{21}P_{20}]^{3+}$ fragment in $In_{37}P_{20}(O_2CR)_{51}$. Second, observations of differential ligand exchange on QDs need not be related to coordination at different facets, but rather may be due to the presence of different and often interlinked coordination networks. As a consequence of this interconnected ligand set, which has predominately bridging binding modes and is free of any neutral, datively bound metal carboxylate complexes, ligand exchange reactions that displace $M(O_2CR)_x$ complexes are likely coupled with significant structural changes. In contrast, X- and L-type ligand exchange reactions can be site specific, allowing for subtle changes to the surface coordination in a controlled manner, as is observed for the reaction of $In_{37}P_{20}(O_2CCH_2Ph)_{51}$ with 1 equiv of water. In addition, spectral line widths of ultrasmall quantum-confined semiconductors may be heavily influenced by lattice vibrations and thus remain broad even for monodisperse samples. Moreover, we hypothesize that the presence of dangling bonds would dramatically influence the electronic structure of these materials and would be readily identified by asymmetry or broadening in the optical spectra.

DOI: 10.1021/jacs.5b13214
J. Am. Chem. Soc. 2016, 138, 1510−1513

■ ASSOCIATED CONTENT

Supporting Information

The Supporting Information is available free of charge on the ACS Publications website at DOI: 10.1021/jacs.5b13214.

Additional details regarding the synthesis, spectroscopic characterization, crystallography, and DFT calculations, including Figures S1−S12 and Tables S1−S5 (PDF)

X-ray crystallographic data for $In_{37}P_{20}(O_2CCH_2Ph)_{51}$ (CIF)

X-ray crystallographic data for $In_{37}P_{20}(O_2CCH_2Ph)_{51}$-$(H_2O)$ (CIF)

■ AUTHOR INFORMATION

Corresponding Author

*cossairt@chem.washington.edu

Notes

The authors declare no competing financial interest.

■ ACKNOWLEDGMENTS

We thank Troy Kilburn for assistance with low-temperature UV−vis measurements. B.M.C. thanks the University of Washington Innovation Award Program and the 3M Non-Tenured Faculty Award Program for generous financial support of this research. This work was facilitated through the use of advanced computational, storage, and networking infrastructure provided by the Hyak supercomputer system at the University of Washington, funded by the Student Technology Fee. X.L. is thankful for financial support from the U.S. National Science Foundation (CHE-1265945 and DMR-1408617).

■ REFERENCES

(1) Lunt, R. R.; Osedach, T. P.; Brown, P. R.; Rowehl, J. A.; Bulović, V. *Adv. Mater.* **2011**, *23*, 5712−5727.

(2) Shirasaki, Y.; Supran, G. J.; Bawendi, M. G.; Bulović, V. *Nat. Photonics* **2013**, *7*, 13−23.

(3) Vossmeyer, T.; Reck, G.; Katsikas, L.; Haupt, E. T. K.; Schulz, B.; Weller, H. *Science* **1995**, *267*, 1476−1479.

(4) Herron, N.; Calabrese, J. C.; Farneth, W. E.; Wang, Y. *Science* **1993**, *259*, 1426−1428.

(5) Schnockel, H. *Chem. Rev.* **2010**, *110*, 4125−4163.

(6) Corrigan, J. F.; DeGroot, M. W., Large Semiconductor Molecules. In *The Chemistry of Nanomaterials: Synthesis, Properties and Applications*, Rao, C. N. R., Muller, A., Cheetham, A. K., Eds.; Wiley-VCH: Weinheim, 2004; Vol. 2, pp 418−451.

(7) Brennan, J. G.; Siegrist, T.; Stuczynski, S. M.; Steigerwald, M. L. *J. Am. Chem. Soc.* **1989**, *111*, 9240−9241.

(8) Beecher, A. N.; Yang, X.; Palmer, J. H.; LaGrassa, A. L.; Juhas, P.; Billinge, S. J. L.; Owen, J. S. *J. Am. Chem. Soc.* **2014**, *136*, 10645−10653.

(9) Jadzinsky, P. D.; Calero, G.; Ackerson, C. J.; Bushnell, D. A.; Kornberg, R. D. *Science* **2007**, *318*, 430−433.

(10) McBride, J. R.; Dukes, A. D. I.; Schreuder, M. A.; Rosenthal, S. J. *Chem. Phys. Lett.* **2010**, *498*, 1−9.

(11) Evans, C.; Guo, L.; Peterson, J.; Maccagnano-Zacher, S.; Krauss, T. *Nano Lett.* **2008**, *8*, 2896−2899.

(12) Gary, D. C.; Terban, M.; Billinge, S. J. L.; Cossairt, B. M. *Chem. Mater.* **2015**, *27*, 1432−1441.

(13) Kudera, S.; Zanella, M.; Giannini, C.; Rizzo, A.; Li, Y.; Gigli, G.; Cingolani, R.; Ciccarella, G.; Spahl, W.; Parak, W. J.; Manna, L. *Adv. Mater.* **2007**, *19*, 548−552.

(14) Wang, Y.; Zhang, Y.; Wang, F.; Giblin, D. E.; Hoy, J.; Rohrs, H. W.; Loomis, R. A.; Buhro, W. E. *Chem. Mater.* **2014**, *26*, 2233−2243.

(15) Yu, Q.; Liu, C.-Y. *J. Phys. Chem. C* **2009**, *113*, 12766−12771.

(16) Zhang, J.; Rowland, C.; Liu, Y.; Xiong, H.; Kwon, S.; Shevchenko, E.; Schaller, R. D.; Prakapenka, V. B.; Tkachev, S.; Rajh, T. *J. Am. Chem. Soc.* **2015**, *137*, 742−749.

(17) Kasuya, A.; Sivamohan, R.; Barnakov, Y. A.; Dmitruk, I. M.; Nirasawa, T.; Romanyuk, V. R.; Kumar, V.; Mamykin, S. V.; Tohji, K.; Jeyadevan, B.; Shinoda, K.; Kudo, T.; Terasaki, O.; Liu, Z.; Belosludov, R. V.; Sundararajan, V.; Kawazoe, Y. *Nat. Mater.* **2004**, *3*, 99−102.

(18) Chan, E.; Xu, C.; Mao, A.; Han, G.; Owen, J.; Cohen, B.; Milliron, D. *Nano Lett.* **2010**, *10*, 1874−1885.

(19) Clark, M. D.; Kumar, S. K.; Owen, J. S.; Chan, E. M. *Nano Lett.* **2011**, *11*, 1976−1980.

(20) Hendricks, M. P.; Campos, M. P.; Cleveland, G. T.; Jen-La Plante, I.; Owen, J. S. *Science* **2015**, *348*, 1226−1230.

(21) Hendricks, M. P.; Cossairt, B. M.; Owen, J. S. *ACS Nano* **2012**, *6*, 10054−10062.

(22) Gary, D. C.; Glassy, B. A.; Cossairt, B. M. *Chem. Mater.* **2014**, *26*, 1734−1744.

(23) Franke, D.; Harris, D. H.; Xie, L.; Jensen, K. F.; Bawendi, M. G. *Angew. Chem., Int. Ed.* **2015**, *54*, 14299−14503.

(24) Xie, R.; Li, Z.; Peng, X. *J. Am. Chem. Soc.* **2009**, *131*, 15457−15466.

(25) Xie, R.; Peng, X. *Angew. Chem., Int. Ed.* **2008**, *47*, 7677−7680.

(26) Murray, C. B.; Kagan, C. R.; Bawendi, M. G. *Annu. Rev. Mater. Sci.* **2000**, *30*, 545−610.

(27) Owen, J. S. *Science* **2015**, *347*, 615−616.

(28) Owen, J. S.; Park, J.; Trudeau, P.-E.; Alivisatos, A. P. *J. Am. Chem. Soc.* **2008**, *130*, 12279−12281.

(29) Adachi, S. *Properties of Group-IV, III-V and II-VI Semiconductors*; John Wiley & Sons: West Sussex, 2005.

(30) Pyykkö, P.; Atsumi, M. *Chem. - Eur. J.* **2009**, *15*, 186−197.

(31) Cros-Gagneux, A.; Delpech, F.; Nayral, C.; Cornejo, A.; Coppel, Y.; Chaudret, B. *J. Am. Chem. Soc.* **2010**, *132*, 18147−18157.

(32) Cossairt, B. M.; Owen, J. S. *Chem. Mater.* **2011**, *23*, 3114−3119.

(33) Kovalenko, M. V.; Scheele, M.; Talapin, D. V. *Science* **2009**, *324*, 1417−1420.

(34) Lan, X.; Masala, S.; Sargent, E. H. *Nat. Mater.* **2014**, *13*, 233−240.

(35) Jennings, W. B.; McCarthy, N. J. P.; Kelly, P.; Malone, J. F. *Org. Biomol. Chem.* **2009**, *7*, 5156−5162.

(36) Micic, O. I.; Curtis, C. J.; Jones, K. M.; Sprague, J. R.; Nozik, A. J. *J. Phys. Chem.* **1994**, *98*, 4966−4969.

(37) Cho, E.; Jang, H.; Lee, J.; Jang, E. *Nanotechnology* **2013**, *24*, 215201.

(38) Narayanaswamy, A.; Feiner, L.; Meijerink, A.; van der Zaag, P. *ACS Nano* **2009**, *3*, 2539−2546.

(39) Murray, C. B.; Norris, D. J.; Bawendi, M. G. *J. Am. Chem. Soc.* **1993**, *115*, 8706−15.

(40) Harris, D. K.; Bawendi, M. G. *J. Am. Chem. Soc.* **2012**, *134*, 20211−20213.

(41) Chen, O.; Wei, H.; Maurice, A.; Bawendi, M.; Reiss, P. *MRS Bull.* **2013**, *38*, 696−702.

(42) Norris, D. J.; Bawendi, M. G. *Phys. Rev. B: Condens. Matter Mater. Phys.* **1996**, *53*, 16338−16346.

(43) Cui, J.; Beyler, A. P.; Coropceanu, I.; Cleary, L.; Avila, T. R.; Chen, Y.; Cordero, J. M.; Heathcote, S. L.; Harris, D. K.; Chen, O.; Cao, J.; Bawendi, M. G. *Nano Lett.* **2016**, *16*, 289.

(44) Cui, J.; Beyler, A. P.; Marshall, L. F.; Chen, O.; Harris, D. K.; Wanger, D. D.; Brokmann, X.; Bawendi, M. G. *Nat. Chem.* **2013**, *5*, 602−606.

(45) Blackburn, J. L.; Ellingson, R. J.; Mićić, O. I.; Nozik, A. J. *J. Phys. Chem. B* **2003**, *107*, 102−109.

(46) Adam, S.; Talapin, D. V.; Borchert, H.; Lobo, A.; McGinley, C.; de Castro, A. R. B.; Haase, M.; Weller, H.; Möller, T. *J. Chem. Phys.* **2005**, *123*, 084706.

(47) Mićić, O. I.; Nozik, A. J.; Lifshitz, E.; Rajh, T.; Poluektov, O. G.; Thurnauer, M. C. *J. Phys. Chem. B* **2002**, *106*, 4390−4395.

DOI: 10.1021/jacs.5b13214
J. Am. Chem. Soc. 2016, 138, 1510−1513